The antimicrobial peptide Defensin cooperates with Tumour Necrosis Factor to drive tumour cell death in *Drosophila*

Jean-Philippe Parvy[1]*, Yachuan Yu[1], Anna Dostalova[2], Shu Kondo[3], Alina Kurjan[5], Philippe Bulet[4], Bruno Lemaitre[2], Marcos Vidal[1] and Julia B. Cordero[1, 5]*

[1] CRUK Beatson Institute, Garscube Estate, Switchback Road, Glasgow, G61 1BD, UK

[2] Global Health Institute, School of Life Sciences, Ecole Polytechnique Federale de Lausanne, Station 19, 1015 Lausanne, Switzerland

[3] Invertebrate Genetics Laboratory, Genetic Strains Research Center, National Institute of Genetics, Mishima 411-8540, Japan

[4] Institute for Advanced Biosciences, CR University Grenoble Alpes, Inserm U1209, CNRS UMR5309, Immunologie Analytique des Pathologies Chroniques, Grenoble, France

[5] Institute of Cancer Sciences, University of Glasgow, Garscube Estate, Switchback Road, Glasgow, G61 1QH, U.K

* Corresponding Authors: j.parvy@beatson.gla.ac.uk, Julia.Cordero@glasgow.ac.uk

Abstract

Antimicrobial peptides (AMPs) are small cationic molecules best known as mediators of the innate defence against microbial infection. While *in vitro* and

26 *ex vivo* evidence suggest AMPs' capacity to kill cancer cells, *in vivo*
27 demonstration of an anti-tumour role of endogenous AMPs is lacking. Using a
28 *Drosophila* model of tumourigenesis, we demonstrate a role for the AMP
29 Defensin in the control of tumour progression. Our results reveal that Tumour
30 Necrosis Factor mediates exposure of phosphatidylserine (PS), which makes
31 tumour cells selectively sensitive to the action of Defensin remotely secreted
32 from tracheal and fat tissues. Defensin binds tumour cells in PS-enriched
33 areas, provoking cell death and tumour regression. Altogether, our results
34 provide the first *in vivo* demonstration for a role of an endogenous AMP as an
35 anti-cancer agent, as well as a mechanism that explains tumour cell sensitivity
36 to the action of AMPs.
37
38
39 **Introduction**
40 Vast amount of evidence demonstrates the key role of systemic
41 immunity in tumour progression and patient outcome. Efforts to manipulate
42 the immune response to tumours are at the core of basic and translational
43 cancer research. In mammals and flies, tumourigenesis triggers inflammation
44 and activation of the immune system, leading to tumour cell death (Cordero et
45 al., 2010; Parameswaran and Patial, 2010; Parisi et al., 2014; Teng et al.,
46 2008). Tumour Necrosis Factor (TNF) is an important player in these
47 tumour/immune interactions and has pleiotropic effects on tumours, including
48 induction of cell death (Ham et al., 2016; Parameswaran and Patial, 2010).
49 This function is conserved in *Drosophila*, where the single TNF homolog Eiger
50 (Egr), produced by tumour-associated macrophages (TAMs), has been shown

51 to drive cell death of neoplastic tumours, generated in larval imaginal discs by
52 the loss of apico-basal complex components such as Disc large 1, Scribble or
53 Lethal giant larvae (Cordero et al., 2010; Parisi et al., 2014; Parvy et al.,
54 2018). Moreover, using *disc large 1 Drosophila* mutant larvae (*dlg*$^{40.2}$ hereafter
55 referred to as *dlg*), we recently reported that tumour-derived Egr, acts on
56 haemocytes to activate Toll pathway in the *Drosophila* fat body, which was
57 necessary to mediate TNF-dependent tumour cell death (Parisi et al., 2014).
58 However, the mechanisms by which Toll signalling activation in immune
59 tissues executes tumour cell death remain unknown (Figure 1A).

60 In *Drosophila* as in mammals, Toll pathway is well known to play a
61 central role in the innate immune response to infection (Lemaitre et al., 1996).
62 Downstream effectors of the Toll pathway include antimicrobial peptides
63 (AMPs), which possess microbicidal activities against various pathogens.
64 They display potent antimicrobial activity *in vitro* by disrupting negatively-
65 charged microbial membranes. While intracellular activities have been
66 reported, many AMPs kill pathogens by inserting into the lipid bilayer and
67 disrupting the membrane integrity (Brogden, 2005). Host cells are instead
68 protected from AMP as they are positively charged and contain cholesterol
69 (Brender et al., 2012). *In vitro* studies have revealed AMPs capacity to kill
70 cancer cells (Deslouches and Di, 2017). However, whether this cancer-killing
71 activity is a natural function of AMPs is unknown, as there are no reports on
72 an *in vivo* paradigm addressing such question. Since the Toll pathway is
73 activated in *dlg* mutant tumour bearing larvae and is required for optimal TNF-
74 induced tumour cell death (Parisi et al., 2014), we hypothesised that AMPs
75 may be involved in this process.

76 Here we show that *Drosophila defensin* is induced in the fat body and
77 tracheal system of *dlg* mutant tumour bearing larvae. We find Defensin
78 consistently associated to dying tumour cells. Critically, systemic and tissue
79 specific knockdown of Defensin demonstrates a non-redundant role of the
80 AMP in controlling tumour growth through the induction of tumour cell death.
81 Anti-tumoural Defensin production relies on TNF-dependent activation of both
82 Toll and Imd pathway. Our results demonstrate that *dlg* mutant tumours
83 expose PS in response to haemocyte-derived TNF and that Defensin is
84 present in PS enriched area on the tumour surface. Finally, we find that lack
85 of TNF prevents PS exposure in tumours and makes them insensitive to the
86 action of Defensin. Collectively, our results reveal an anti-tumoural role for
87 Defensin *in vivo* and provide insights into the molecular mechanisms, which
88 make tumours sensitive to the killing action of an endogenous AMP.
89

90 **Results**

91 ***dlg* tumour bearing larvae express the AMP Defensin**

92 In order to assess expression of several AMPs we performed RT-
93 qPCR analysis on fat bodies dissected from wild type controls (w^{1118}) or *dlg*
94 mutant larvae (Figure 1B). Results showed consistent and statistically
95 significant upregulation of *defensin* in fat bodies of *dlg* larvae compared to
96 wild-type ones (Figure 1B). Other Toll-dependent AMPs display a trend to be
97 increased (*drosomycin* and *attacin A*), even though data was highly variable
98 amongst biological replicates, while other AMPs were not transcriptionally
99 regulated (*drosocyn*, *cecropin A1*) (Figure 1B). Interestingly, human β-
100 Defensin 1 displays anticancer activity *in vitro* (Bullard et al., 2008; Sun et al.,

101 2006), and deletion of human *def* appears prevalent in some cancer types (Ye
102 et al., 2018). This prompted us to explore the role of *Drosophila* Defensin in
103 *dlg* mutant tumours. Using *dlg* larvae reared on antibiotics, we confirmed that
104 *defensin* upregulation was independent of the presence of microbes (Figure
105 1C). Moreover, larvae bearing *dlg* imaginal discs tumours induced by RNAi
106 (*en>UAS-dcr2; UAS-dlg-IR*) also displayed increased *defensin* expression,
107 confirming AMP gene induction as a consequence of *dlg*-driven epithelial
108 transformation rather than whole body gene loss (Figure 1D). We conclude
109 that Defensin, an AMP known for its activity against microbes, is induced, in a
110 sterile environment, by the presence of tumours.
111
112 **Defensin restrains *dlg* tumour growth and promotes tumour cell death.**
113 We next hypothesized that Defensin may be an important mediator of
114 anti-tumour immunity *in vivo*. To test this hypothesis, we generated null
115 mutant alleles for the *defensin (def)* gene using the CRISPR/Cas9 system
116 (def^{sk3} and def^{sk4}) (Figure 1E) (Hanson et al., 2018). Survival analysis of def^{sk3}
117 flies confirmed that this AMP contribute to resist systemic infection to certain
118 Gram-positive bacteria (Figure supplement 1) (Levashina et al., 1995). To
119 evaluate the effect of Defensin on tumour development, we combined *def* and
120 *dlg* loss of function alleles. Compared to *dlg* mutant animals, *dlg;def* double
121 mutants displayed a significant increase in tumour size (Figure 2A). Tumour
122 growth is limited by apoptotic tumour cell death as revealed by Dcp1 staining
123 (Parisi et al., 2014). Interestingly, tumours from *dlg;def* double mutants display
124 a very strong decrease in apoptosis (Figure 2B-E'), suggesting that increased
125 tumour size in absence of Defensin is due to a decrease in tumour cell death.

126 This was further supported by the similar proliferation rates measured in *dlg*
127 and *dlg,def* mutant tumours as per quantification of anti-phophoHistone H3
128 staining (Figure supplement 2A-E'). Importantly, the effect of Def on tumour
129 size and cell death were still observed when *dlg* and *dlg,def* larvae were
130 reared in sterile conditions (Figure supplement 2F-J') and further confirmed
131 upon ubiquitous knock down of *def* using RNA interference (IR) (Figure 2F-J').
132 Furthermore, fat body overexpression of *def* significantly rescued tumour
133 volume and tumour cell death of *dlg;def*^{sk3} double mutant animals (Figure 2K
134 and L). Additionally, larval injection of a synthetic Defensin peptide increased
135 tumour cell death of *dlg* or *dlg;def*^{sk3} imaginal discs (Figure 2M), while it had
136 no effect on tissues from wild-type larvae, indicating that Defensin can
137 selectively promote cell death of tumour cells. Altogether, these results
138 demonstrate that Defensin is required to control *dlg*-dependent
139 tumourigenesis *in vivo* through induction of tumour cell death.
140

141 **Defensin remotely produced from immune tissues bind to tumour cells**

142 Having shown that Defensin restrict tumour growth, we sought to
143 determine the tissues that produced endogenous Defensin in the context of
144 tumour bearing. Previous studies have shown that Defensin is not produced
145 by imaginal discs or tumours (Bunker et al., 2015; Kulshammer et al., 2015).
146 In the context of infection, Defensin can be produced by the fat body as well
147 the tracheal and gut epithelium (Tzou et al., 2000). We monitored *defensin*
148 expression by RT-qPCR in various immune tissues of tumour bearing
149 animals. We observed that the fat body, homologue to the mammalian liver
150 and adipose tissue, and the trachea, a network of tubes transporting oxygen

151 to cells that resembles the mammalian vasculature, were the main sources of
152 *defensin* in these animals (Figure 3A). This was also supported by Defensin
153 immunostaining, (Figure 3B and C). Transcript assessment upon targeted IR
154 knock down of *defensin* in the respective tissues further confirmed the
155 domains of endogenous gene expression (Figure 3D and I). Importantly,
156 knocking down *defensin* expression specifically in the fat body or the trachea
157 of *dlg* animals, resulted in increased tumour size and decreased tumour cell
158 death (Figure 3E-H' and J-M') confirming the non-redundant functional
159 requirement of *defensin* in both tissues to efficiently promote tumour cell
160 death.

161 To investigate the possibility that Defensin produced by the fat body
162 and the trachea can specifically target tumour cells, we made use of an
163 inducible haemagglutinin (HA) tagged form of Defensin (*UAS-def-HA*). We
164 noticed leaky HA protein expression in the tracheal system (Figure 4A) but not
165 in the fat body (Figure 4B) of animals carrying the *UAS-def-HA* construct only.
166 Therefore, we overexpressed *UAS-def-HA* in the fat body using a Gal4
167 specific driver (*lpp>def-HA*), which resulted in significant upregulation of
168 Defensin in the fat body (Figure 4D) when compared to control conditions
169 (Figure 4B), but also maintained the leaky expression of the transgene in the
170 trachea (Figure 4C). Strikingly, overexpression of *UAS-def-HA* in the fat body
171 resulted in Defensin-HA immunostaining in transformed imaginal discs from
172 *dlg* mutant animals (Figure 4E and E') but not in normal tissues from *dlg*
173 heterozygous animals (Figure 4F and F').

174 Consistently, using anti-Defensin antibody, we observed endogenous
175 Defensin staining on *dlg* mutant tumour (Figure 4G-H'') but not in the wild-type

176 discs (Figure 4I). Interestingly, we predominantly observed Defensin bound to
177 tumour areas enriched with apoptotic cells (Figure 4H-H''). High-resolution
178 imaging showed Defensin enrichment at the membrane of these dying cells
179 (Figure 4J-J'').

180 Altogether, these results show that Defensin produced by immune
181 tissues selectively binds tumour cells to target them for apoptosis.

182

183 **Toll and Imd pathway contribute to Defensin expression in *dlg* mutant**
184 **larvae**

185 *defensin* expression upon systemic infection relies on both Toll and
186 Imd pathways (Lemaitre et al., 1996; Leulier et al., 2000). While we previously
187 showed that Toll pathway activation in *dlg* mutant larvae is required to achieve
188 maximal tumour cell death (Parisi et al., 2014), the involvement of the Imd
189 pathway in tumour bearing animals was still elusive. To assess the
190 contribution of the Imd pathway to both *defensin* expression and tumour
191 burden, we analysed these two phenotypes in larvae deficient for the Imd-
192 pathway. We observed a 55-60% decrease in *defensin* expression in *dlg*
193 mutants carrying a loss of function allele affecting *imd* (*dlg;imd*^{1}) (Figure 5A)
194 or the gene encoding the downstream transcription factor Relish (*dlg;rel*^{E20})
195 (Figure 5F). Consistently, analysis of tumour phenotypes revealed increased
196 tumour volume and decreased tumour cell death in *dlg;imd*^{1} and *dlg;rel*^{E20}
197 animals when compared with *dlg* counterparts (Figure 5B-E' and G-J').
198 Altogether, these data demonstrate that the Imd pathway is required for
199 *defensin* upregulation, impairment of tumour growth and induction of tumour
200 cell death in *dlg* mutant larvae.

201 Upon infection, AMP expression in the trachea exclusively relies on the
202 Imd pathway (Tzou et al., 2000). We therefore looked at *defensin* expression
203 and tumour phenotype in *dlg* mutant larvae where *imd* expression had been
204 knocked down specifically within tracheal cells (*dlg;btl>imd-IR*). In this setting,
205 *defensin* expression was significantly reduced in the whole larvae (Figure 6A).
206 Consistently, tumour volume was increased while tumour cell death was
207 decreased (Figure 6B-E') showing the requirement of Imd pathway in the
208 tracheal system to control tumour burden.

209 In the fat body, both Imd and Toll patways contribute to AMPs
210 expression during infection (Tzou et al., 2002). To evaluate the contribution of
211 Toll and Imd pathways in fat body in tumour bearing larvae, we monitored
212 *defensin* expression and tumour phenotype in *dlg* animals in which Toll or Imd
213 pathways have been selectively knocked down in the fat body. Knocking
214 down *myd88,* which encodes a common adaptor to Toll receptors (Imler and
215 Zheng, 2004), or *imd* in the fat body resulted in a significant decrease in
216 *defensin* expression (Figure 6F) and, consistently, increased tumour volume
217 and decreased tumour cell death (Figure 6G-K'). Moreover, concomitant
218 overexpression of *defensin* and *Myd88-IR* or *Imd-IR* in the fat body of *dlg*
219 larvae was sufficient to significantly rescue the tumour volume and tumour cell
220 death phenotypes resulting from fat body knockdown of *Myd88* or *Imd* in *dlg*
221 animals (Figure 6L-O).

222 We conclude that, in *dlg* mutant animals, Toll and Imd pathways have
223 non-redundant roles in restricting tumour growth and promoting tumour cell
224 death through the control of *defensin* expression. Importantly, forced Defensin

225 expression in an otherwise immune-compromised animal is sufficient to
226 reduce tumour growth and to promote tumour cell death.
227
228 **Defensin is enriched in tumour areas exposing phosphatidylserine**
229 AMPs targeting of pathogens, involves the recognition of negatively
230 charged molecules exposed on the cell surface (Yeaman and Yount, 2003). A
231 key question raised by our study is how Defensin can selectively bind and kill
232 tumour cells (Figure 4 and Figure 2M). Selective action of cationic AMP is
233 attributed to their ability to interact with negative charged membrane such as
234 those found in bacteria. We hypothesized that the membrane of tumour cells
235 from *dlg* mutant larvae might change their electrostatic properties, making
236 them sensitive to the action of Defensin. Phosphatidylserine **(**PS) is a
237 negatively charged phospholipid, normally restricted to the inner leaflet of the
238 cell membrane. However, PS can be exposed on the outer leaflet for example
239 in apoptotic cells, which tags these cells for phagocytosis (Birge et al., 2016;
240 Shklyar et al., 2013; Tung et al., 2013). Moreover, PS exposure has been
241 shown to occur independently of apoptosis in many cancer cell types (Riedl et
242 al., 2011). Therefore, we investigated whether PS externalisation could be a
243 factor allowing specific targeting of tumour cells by Defensin. Our data
244 revealed that *dlg* but not wild-type tissues, displayed high levels of Annexin V
245 staining (Figure 7A and B), indicating increased exposure of PS by *dlg*
246 tumours. We next looked at the ability of Defensin to specifically associate
247 with tumour cells exposing PS and found that Defensin localized in PS-
248 enriched areas on *dlg* tumours (Figure 7A-A''). Thus, Defensin produced by

249 immune responsive tissues binds specifically to tumour cells and this ability
250 correlated with the exposure of PS.
251
252 **The TNF homolog Eiger is required for PS exposure and Defensin anti-**
253 **tumoural activity.**
254 Previous studies have shown that circulating macrophage-like cells in
255 *Drosophila,* called haemocytes, bind to *dlg* mutant tumours and contribute to
256 cell death (Parisi et al., 2014). This process is mediated by the release of
257 Eiger from haemocytes (Cordero et al., 2010; Parisi et al., 2014), which then
258 activates the JNK pathway in target cells to promote apoptosis (Igaki et al.,
259 2009). Moreover, Toll pathway–activation in tumour bearing animals also
260 requires Eiger (Parisi et al., 2014). Accordingly, we found that *defensin*
261 upregulation observed in *dlg* animals was lost in *dlg;egr*^{3} double mutants
262 (Figure 7C). We next tested whether PS exposure in tumours was dependent
263 on Eiger, and observed an almost complete loss of cell-surface PS in *dlg;egr*^{3}
264 tumours (Figure 7A, D and E). Therefore, Eiger is required for PS exposure in
265 these tumours. We then analysed PS exposure in *dlg* mutant tumours, upon
266 specific *eiger* knockdown in haemocytes (*dlg;hml>egr-IR*), and observed a
267 strong decrease in cell surface-exposed PS compared to control tumours
268 (*dlg;hml>ctrl-IR*) (Figure 7F-H). This indicates that PS exposure in tumour
269 cells is likely triggered by the release of Eiger from haemocytes.
270 Importantly, Egr-dependent signalling and PS exposure were intact in *dlg;def*
271 and *dlg;imd* mutants (Figure 7I-L and Figure supplement 3). This indicates
272 that Eiger signalling and PS exposure precedes the action of Defensin in *dlg*
273 tumours. To further assess whether Eiger was required for Defensin-induced

274 tumour cell death, we injected synthetic Defensin peptide into control, *dlg* or
275 *dlg;egr*^{3} mutant larvae. As expected, Defensin injection was able to robustly
276 promote tumour cell death in *dlg* mutant tumours (Figure 7M). However,
277 Defensin was unable to affect tumours derived from Eiger -deficient animals,
278 demonstrating the requirement of Eiger for tumour cell death induced by
279 Defensin (Figure 7M).
280

281 **Discussion**

282 While the role of antimicrobial peptides in innate immune defense has been
283 well-recognized for decades (Bahar and Ren, 2013), recent reports revealed
284 potential additional physiological functions of AMPs, including aging and
285 neurodegeneration (Cao et al., 2014; Kounatidis et al., 2017; Lezi et al.,
286 2018), wound-healing (Chung et al., 2017; Tokumaru et al., 2005), resistance
287 to oxidative stress (Mergaert et al., 2017; Zhao et al., 2011), immune signaling
288 (Tjabringa et al., 2003; van Wetering et al., 2002) and anti-cancer activity
289 (Deslouches and Di, 2017). However, due to the absence of AMP mutants,
290 most of these studies have relied on the use of exogenous sources of AMPs
291 or genetic modification of upstream regulators of AMP expression. Recently,
292 the use of loss of function alleles of *Drosophila* Diptericin (DptB), allowed to
293 establish a role for the AMP in long-term memory (Barajas-Azpeleta et al.,
294 2018). Pioneer work reporting systematic deletion of multiple AMPs in
295 *Drosophila*, opens the door for in-depth analysis of the endogenous functions
296 of these molecules (Hanson et al., 2018). Using such tools and a genetically
297 defined *in vivo* tumour model, our study demonstrates a role for Defensin in
298 the control of tumours and deciphers the molecular mechanism allowing

299 specific tumour cell targeting by the AMP. Collectively, our results suggest a
300 model of tumour control in two steps: Firstly, the cellular immune response to
301 tumours involves the binding of haemocytes to tumour cells and activation of
302 TNF pathway leading to PS exposure (Figure 7N). This is followed by a
303 humoral response achieved by the action of antimicrobial peptides remotely
304 produced by the fat body and the trachea (Figure 7N). Thus, the two branches
305 of *Drosophila* innate immunity contribute to tumour elimination.
306

307 **A role for a *Drosophila* AMP in tumour control**

308 Using mutants as well as ubiquitous or targeted knockdowns, our study
309 reveals that Defensin is non-redundantly required to drive tumour cell death
310 and restrict tumour growth in neoplastic tumours generated by loss the apico-
311 basal determinant Dlg. This was reinforced by detection of Defensin on dying
312 tumour cells as well as genetic rescue and injection experiments showing that
313 Defensin can actively drive tumour cell death. Several *in vitro* studies in
314 mammals have pointed to AMPs anti-tumoural potential (Deslouches and Di,
315 2017). Amongst these suggested anticancer peptides, Human β-Defensin 1
316 (hBD1) appears downregulated in 82% of prostate cancer and 90% of renal
317 clear cell carcinomas (Donald et al., 2003). Furthermore, expression of hBD1
318 induces cell death in prostate and renal cancer cells *in vitro* (Bullard et al.,
319 2008; Sun et al., 2006). Moreover, a recent report shows prevalent deletion of
320 Human *defensin* gene cluster in some tumour types including prostate, lung
321 and colorectal cancers, as well as a decrease overall survival in patients
322 carrying these deletions (Ye et al., 2018). However, since the classification of
323 a molecule as AMP is based on structural protein features, it is important to

324 mention that Human Defensins are not homologous of, but rather have
325 structural resemblances, to *Drosophila* AMPs due to convergent evolution
326 (Shafee et al., 2017). Further studies are required to determine if anticancer
327 activity displayed by Defensins from different species is linked to their
328 structural properties.

329 As upon infection (Tzou et al., 2000), we show that the fat body and the
330 trachea are the main sources of Defensin in tumours bearing larvae.
331 Moreover, our results indicated that Defensin's maximal expression, and anti-
332 tumour properties rely on Imd and Toll pathways activation. As expected from
333 previous studies on anti-pathogenic immunity, Imd appears to play a critical
334 role in the tracheal system, while both Imd and Toll drive Defensin expression
335 in the fat body (Hoffmann and Reichhart, 2002; Tzou et al., 2002).
336 Consistently, overexpressing Defensin partially rescued the effect of Imd or
337 Toll knockdown on *dlg* tumours. However, Toll and Imd pathways are major
338 regulators of multiple AMPs in the *Drosophila* fat body. Then, it is conceivable
339 that AMPs other than Defensin may possess similar anti-tumoural activity. In
340 fact, a recent study in *Drosophila* shows that ectopic expression of several
341 antimicrobial peptides, including the Defensin, can increase cell death in a
342 haematopoietic tumour model (Araki et al., 2018). Authors of that study also
343 reported activation of Toll and Imd pathways together with increased
344 expression of several AMPs in those tumour bearing animals. Together with
345 our study, this suggests potentially general anti-tumoural properties of
346 *Drosophila* AMPs.

347

348 **Defensin specifically targets tumour cells**

349 Importantly, we show that Defensin targets tumour cells for apoptosis
350 while sparing normal cells. As their human counterparts, we show that
351 *Drosophila* tumours can expose PS independently of cell death (Riedl et al.,
352 2011). Interestingly, an *in vitro* study showed selective anticancer activity of
353 some synthetic peptides derived from beetle Defensin, against cancer cells
354 exposing PS (Iwasaki et al., 2009). A similar targeting mechanism has also
355 been proposed to explain temporin-1CEa or L-K6 anticancer activities towards
356 melanoma cells and breast cancer cells respectively (Wang et al., 2016;
357 Wang et al., 2017). PS is a mark of apoptotic cells, which is used as an "eat
358 me" signal by phagocytes (Shklyar et al., 2013; Tung et al., 2013). In
359 *Drosophila*, the phagocytic receptor Simu together with Draper contribute to
360 the elimination of apoptotic to the recognition of PS (Shklyar et al., 2013; Tung
361 et al., 2013). It would be interesting to test the role of these receptors in the
362 control of *dlg* tumour progression.

363 Our results indicate that PS exposure precedes Defensin action and is
364 not just an "eat-me" signal but likely contributes to changing the membrane of
365 tumour cells making them sensitive to the action of AMPs. It is tempting to
366 speculate that deleterious effect of AMPs observed upon aging or
367 neurodegeneration may involve a similar targeting mechanism of 'foreign-
368 looking' or unfit cells (Cao et al., 2013; Kounatidis et al., 2017; Lezi et al.,
369 2018).

370 Noteworthy, other negatively charged molecules enriched on tumour
371 surface such as heparan sulfates and O-glycosylated mucins may also
372 contribute to the targeting by AMPs (Hollingsworth and Swanson, 2004;
373 Knelson et al., 2014).

374

375 **Defensin action requires TNF**

376 TNF is a major player in the tumour microenvironment by exerting
377 pleiotropic effects on both the tumour and its surroundings (Ham et al., 2016;
378 Parameswaran and Patial, 2010). In our *dlg* mutant model, we observed that
379 defensin induction requires TNF, supporting previous observations that
380 induction of innate immune response in tumour bearing animal relied on Eiger
381 produced by the tumour (Parisi et al., 2014). Indeed, Toll activation in the fat
382 body has been proposed to be a consequence of tumour-derived TNF, which
383 drives haemocyte proliferation leading to an increase in Toll ligand Spatzle
384 (Parisi et al., 2014). Whether Imd pathway is also indirectly activated by the
385 changes in immune cell activity in response to tumour or by alternative
386 mechanisms remains an open question.

387 Our results show that haemocyte-derived TNF is required for PS
388 exposure by the tumour, a key process for tumour targeting by Defensin.
389 Consistently, haemocyte-derived TNF is shown to drive cell death in *dlg*
390 mutant tumours (Parisi et al., 2014). The precise molecular mechanisms
391 driving PS exposure downstream of TNF remain unknown. However,
392 haemocyte-derived TNF, activates JNK pathway, which triggers many
393 changes in tumour cells including apoptosis (Igaki et al., 2002; Moreno et al.,
394 2002), ROS production (Fogarty et al., 2016; Santabarbara-Ruiz et al., 2015),
395 loss of cell polarity (Zhu et al., 2010), modification of extracellular matrix
396 (Uhlirova and Bohmann, 2006), proliferation and cell migration (Beaucher et
397 al., 2007; Igaki et al., 2006; Pastor-Pareja et al., 2004; Srivastava et al.,
398 2007). Thus, TNF might also sensitize cells through activation of the JNK

399 pathway (Cordero et al., 2010) providing, in addition to PS exposure, a
400 secondary sensitization mechanism of tumour cells to the action of the AMP.
401 Further studies are needed to explore a potential link between JNK activation
402 and PS exposure since pleiotropic effects of JNK may drive PS exposure
403 downstream of TNF.

404 Another consequence of TNF-dependent JNK activation in tumours is
405 the increased expression of matrix metalloproteases (Mmps) by tumour cells
406 (Uhlirova and Bohmann, 2006). Importantly, we show that Mmp-1 induction
407 and then JNK pathway activation are still present in tumour from larvae
408 devoided of Defensin. This demonstrates that TNF signalling acts upstream of
409 Defensin. Mmps degrade the basal membrane facilitating metastasis of
410 primary tumour cells (Beaucher et al., 2007; Pastor-Pareja et al., 2004;
411 Srivastava et al., 2007). Interestingly, a study reported that human Mmp-7 can
412 cleave immature Defensins, promoting their activation (Wilson et al., 1999;
413 Wilson et al., 2009). Indeed, the pro-domain present in AMPs is thought to
414 keep their *in vivo* activity silent, allowing local activation of AMP upon
415 cleavage. While the mechanisms of *Drosophila* Defensin pro-domain
416 cleavage remain unknown, it would be interesting to explore whether the
417 changes in the tumour microenvironment could also affect Defensin
418 activation.

419

420 In conclusion, our study provides the first direct *in vivo* demonstration of the
421 role of an endogenous AMP as an anti-cancer agent in *Drosophila*. Our data
422 points to a conserved mechanism of tumour control by AMPs, a potent arm of
423 the innate immune system. Importantly, we identify cellular features within

424 tumours, which may be predictive of their sensitivity to be targeted by AMPs.
425 This study provides a new paradigm to decipher the molecular mechanisms
426 influencing anti-tumoural functions of an AMP, which may extend to other
427 non-canonical roles of AMPs, such as in ageing, long-term memory and
428 wound healing. Moreover, together with the new genetic tools allowing
429 targeting of all *Drosophila* AMPs (Hanson et al., 2018), our study establishes
430 new bases to explore *in vivo* a potential important natural mechanism of
431 defence against tumours.
432

433 **Material and Methods**

434 ***Drosophila* housekeeping and rearing**

435 Flies were reared at 25°C under 12h/12h light/dark cycles on standard
436 oatmeal and molasses medium (Fernandez-Ayala et al., 2009). Details on fly
437 strains used in this study are presented in Table supplement 1 and detailed
438 genotypes are included in corresponding figure legends.

439 For assessment of tumour volume and tumour cell death, flies were
440 transferred to medium embryo collection cages and allowed to lay eggs for 8h
441 at room temperature (RT) on agar/grape juice plates (2.1% agar, 25% grape
442 juice, 1.25% sucrose, 0.2% methyl 4-hydroxybenzoate) supplemented with
443 yeast paste. Plates were kept at 25°C until hatching. 200 larvae hatched
444 within a 4h time window were collected and transferred to rearing bottles
445 containing 45mL of fly food to avoid any developmental delay and/or
446 starvation effects due to overcrowding conditions. The tumour phenotype was
447 analysed close to the normal developmental time, i.e. 7 days after hatching.
448 Tumours were dissected and stained for further analysis (see below).

449

450 **Generation of *defensin* mutants**

451 *def*^{sk3} and *def*^{sk4} mutants were generated using CRISPR/cas9
452 technology (Hanson et al., 2018). Mutants were isogenized through
453 backcrosses with a *w*^{1118} *iso* line as previously described in Ferreiera-Teixeira
454 et al, 2014.

455

456 **Survival assays**

457 Survival of *def*^{SK3} animals was compared to wild type controls
458 (isogenised background, *iso*). Male flies (5-7 days old) were pricked in the
459 thorax with a needle dipped in a concentrated pellet of fresh overnight
460 bacterial culture. Infected flies were kept at 29°C. *Listeria innocua* was
461 cultured in Brain heart infusion medium at 37°C and used at optical density of
462 200nm (OD_{600}). *Erwinia carotovora carotovora 15* was cultured in Luria-
463 Bertani broth at 29°C and used at OD_{600} 200. Experiments were repeated
464 three times independently and one representative experiment is shown.

465

466

467 **Immunohistochemistry**

468 Tissues were dissected in Phosphate Buffer Saline (PBS) and fixed for
469 20min in 4% formaldehyde. Fat body samples were fixed for 30min using the
470 same protocol. Tissues were washed three times in PBS containing 1% of
471 Triton-X100 (PBT) and incubated overnight at 4°C with primary antibodies.
472 Tissues were washed 5 times in PBT and incubated for 2h at RT with
473 secondary antibodies and 4',6-Diamidine-2′-phenylindole dihydrochloride

474 (DAPI, Sigma) (1µg/mL). After three washes in PBT, tissues were mounted in
475 Vectashield (Vector Laboratories, Inc.) using Secured-Seal spacers (Thermo
476 Fisher Scientific).

477 The following primary antibodies and corresponding dilutions were
478 used: rabbit anti-Dcp1 (1/100), rabbit anti-phosphoHistone H3 (ser10 and
479 ser28 mixed, 1/100) and mouse anti-HA (1/1000) (Cell Signalling
480 Technology); mouse anti-Mmp1 (1/10) (Developmental Studies Hybrydoma
481 Bank, 3B8D12); chicken anti-GFP (1/4000) Abcam) and guinae pig anti-
482 Defensin (1/100) (Kind gift from Dahua Chen, (Ji et al., 2014)). Secondary
483 goat antibodies were Alexa Fluor® 488nm or 594nm (Invitrogen) conjugated
484 and were used at 1/500 dilution.

485 Confocal images were captured using a Zeiss 710 or Zeiss 880 with
486 Airyscan confocal microscope and processed with Fiji 2.0.0 or Adobe
487 Photoshop C.S5.1.

488

489 **Quantification of tumour volume and tumour cell death**

490 For analysing tumour phenotype, images were acquired using optimal
491 slice parameter and 12bits using a Zeiss 710 confocal microscope.
492 Quantifications were made as previously described (Parisi et al., 2014).
493 Briefly, we used Volocity 3D imaging analysis software (Perkin Elmer) to
494 quantify the total volume of tumour identified by DAPI staining and cell death
495 visualised with anti-Dcp1 staining. When haltere or leg discs tumours were
496 still associated with the wing disc, they were not considered for quantification.
497 Quantifications were done in at least three independent biological replicates
498 for each genetic setting. Single representative experiments are presented

499 except for *dlg;def* double mutant rescue experiments (Figure 1L-M) for which
500 replicates are pooled due to the few larvae available. In all cases the
501 difference between control and mutant tumour were strongly reproducible
502 between replicates.
503
504 **Sterile rearing conditions**
505 To rule out any effect of infection on the tumour phenotypes,
506 *Drosophila* larvae were reared on standard food supplemented with penicillin
507 and streptomycin (100 IU/ml and 100 mg/ml, respectively) (Figure 1A, Figure
508 supplement 3A-E' and Figure supplement 4G).
509
510 **qRT-PCR analysis**
511 Total RNA from 7 to 10 whole larvae or tissues collected from 10 to 20
512 larvae (10 larvae for fat body, 20 larvae for trachea) was extracted using
513 TRIzol (Thermo Fisher Scientific), according to the manufacturer's
514 instructions. RNA was treated with Turbo DNA free Kit (Life Technologies
515 LTD) and RNA concentration and quality were monitored using a Nanodrop
516 (Thermo Fisher Scientific). The same amount of total RNA (1µg for whole
517 larvae and fat body or 100ng for trachea) was used to perform the three
518 independent reverse-transcriptions using the High-Capacity cDNA Reverse
519 Transcription Kit (Applied Biosystems). cDNAs were pooled and qPCR was
520 performed using PerfeCTa SYBR green (Quanta Bio), following the
521 manufacturer's instructions. cDNA amplification was monitored with Applied
522 Biosystems 7500 fast instruments. Serial 10-fold dilutions of an external
523 standard were used to produce a standard curve, and RNA samples were

524 included to control for the absence of DNA contamination. *rpl32* expression
525 was used to normalize expression levels of target genes. Data was analysed
526 using the Ct method ($2^{-\Delta\Delta ct}$). All qPCR experiments were carried out on three
527 to seven independent biological replicates (see figure legends for details) and,
528 larvae were sampled from the same bottle used to analyse the tumour
529 phenotype. GraphPad Prism7 software was used for graphical representation
530 and statistical analysis. Primer targets and sequences are presented in Table
531 supplement 2.
532
533 **PCR amplification of genomic DNA**
534 To verify the sequence of *def*^{sk3} and *def*^{sk4} mutants, genomic DNA was
535 extracted from single flies by grinding whole animals with a 200µL pipette tip
536 containing 50µL of squishing buffer (10mM Tris-HCl pH 8.2, 1mM EDTA,
537 25mM NaCl, 200µg proteinase K) followed by incubation at 37°C for 30min.
538 Proteinase K was heat-inactivated at 95°C for 2min. 1µL of genomic DNA was
539 used for PCR amplification using PfuUltra II Fusion DNA Polymerase (Agilent)
540 (for primers see Table supplement 2) and Eppendorf Mastercycler Ep
541 Gradient Thermal Cycler.
542
543 **Annexin V staining and quantification**
544 Tumours were dissected in PBS and incubated in Annexin V binding
545 buffer (Fisher Scientific) containing 5% of Alexa Fluor (488nm or 568nm)
546 conjugated Annexin V (Life Technologies LTD) for 10min. Tissues were
547 washed quickly in Annexin V binding buffer and fixed in 4% formaldehyde for

548 20min. Immunostaining, mounting and imaging were then carried out as
549 described above.
550 We used Fiji 2.0.0 software to quantify Annexin V staining at the
551 tumour surface. Maximal Z-projection of whole tumours were generated and
552 the Colour Threshold tool was then used to detect the red pixels that
553 represented Annexin V staining at the surface of tumours. The hue slider was
554 set to include only the red signal, and the brightness slider was adjusted to
555 exclude any background signal. This area was then selected and measured in
556 pixels.
557
558 **Synthetic Defensin production and injections**
559 The mature Defensin peptide
560 (ATCDLLSKWNWNHTACAGHCIAKGFKGGYCNDKAVCVCRN) was
561 synthesised (over 90% purity) and the purity controlled by Genepep using
562 Ultra Performance Liquid Chromatography/ Mass Spectrometry. We
563 subsequently compared the integrity of synthetic Defensin with authentic
564 Defensin purified from *Drosophila* hemolymph using two complementary
565 approaches, namely Matrix-Assisted Laser Desorption/Ionization-Mass
566 Spectrometry (MALDI-MS) for molecular mass determination and trypsin
567 digestion followed by nanoLiquid Chromatography/Electrospray Ionization
568 tandem Mass Spectroscopy (nano*LC/ESI MS/MS*) for molecular integrity
569 confirmation. Those analyses confirmed the similar mass between natural and
570 synthetic Defensin (respectively provided by Bulet EIRL and Genepep) as well
571 the presence of disulphide bonds within synthetic Def, demonstrating it is the
572 mature peptide (Data not shown).

573 For injection experiments, larvae were collected, washed three times in
574 cold sterile PBS and injected on a fly pad (Flystuff-SLS UK) upon CO_2
575 anaesthesia using Nanoject II and glass capillaries 3.5 inch (Drummond).
576 Larvae were injected with 69nL of PBS containing 7.5nmol of synthetic
577 Defensin or 69nL of PBS only as control. Larvae were then gently transferred
578 into agar/grape juice plates and kept at 25°C. Tumours were dissected 4h
579 after injection and stained for visualization of nuclei and tumour cell death as
580 describe above.
581
582 **Statistical analyses**
583 All data are presented as mean ± SD and n values are indicated in the
584 figure legends. Statistical analyses were carried out using GraphPad Prism7
585 software and only significant differences are indicated in dot-plots. Survival
586 upon infection was analysed using Log-rank test. qPCR data were analysed
587 using unpaired t-test with a two-tailed p value. Tumour volume and tumour
588 cell death comparing 2 samples were analysed using Mann-Whitney test with
589 a two-tailed p value and the one comparing 3 genotypes were analysed using
590 One-way ANOVA followed by Turkey's multiple comparisons test. Tumour
591 volume from injected larvae was analysed using Two-way ANOVA followed by
592 Turkey's multiple comparisons test and only significant statistical differences
593 between ctrl and Defensin injected larvae for each genotype tested are
594 indicated.
595
596 **Acknowledgments:** We would like to thank Dr. Dahua Chen for the anti-
597 Defensin antibody, the Vienna *Drosophila* Resource Centre and the

598 Bloomington *Drosophila* Stock Centre for fly stocks, and Dr. Sébastien Voisin
599 for his critical contribution in mass spectrometry analyses. JPP and YY are
600 supported by Cancer Research UK core funding through the CRUK Beatson
601 Institute (A17196). JBC is a Sir Henry Dale Fellow jointly funded by the
602 Wellcome Trust and the Royal Society (grant number 104103/Z/14/Z). *In*
603 *memory of Marcos Vidal (1974-2016).*
604
605
606 **Author contributions:** MV initiated this project. JPP performed most of the
607 experiments in this study; YY and AK provided technical assistance; AD
608 assayed fly survival upon infection; SK and BL generated the *defensin* mutant
609 flies; PB analysed the quality of synthetic Def; JPP and JBC designed
610 experiments and analysed the data; BL provided important insights into AMPs
611 and *Drosophila* immunity; JPP, PB, BL and JBC wrote the paper; JBC
612 directed the study.
613
614 **Competing interests:** Authors declare no competing interests.
615
616 **Data and material availability:** All data and materials supporting the findings
617 of this study are available from the corresponding authors upon request.
618
619

620 **References**

621 Araki, M., Awane, R., Sato, T., Ohkawa, Y., and Inoue, Y. (2018). Anti-tumor effects
622 of antimicrobial peptides, targets of the innate immune system, against
623 hematopoietic tumors in Drosophila mxc mutants. BioRxiv.
624 Bahar, A.A., and Ren, D. (2013). Antimicrobial peptides. Pharmaceuticals (Basel)
625 *6*, 1543-1575.
626 Barajas-Azpeleta, R., Wu, J., Gill, J., Welte, R., Seidel, C., McKinney, S., Dissel, S., and
627 Si, K. (2018). Antimicrobial peptides modulate long-term memory. PLoS Genet
628 *14*, e1007440.
629 Beaucher, M., Hersperger, E., Page-McCaw, A., and Shearn, A. (2007). Metastatic
630 ability of Drosophila tumors depends on MMP activity. Dev Biol *303*, 625-634.
631 Birge, R.B., Boeltz, S., Kumar, S., Carlson, J., Wanderley, J., Calianese, D., Barcinski,
632 M., Brekken, R.A., Huang, X., Hutchins, J.T.*, et al.* (2016). Phosphatidylserine is a
633 global immunosuppressive signal in efferocytosis, infectious disease, and cancer.
634 Cell Death Differ *23*, 962-978.
635 Brender, J.R., McHenry, A.J., and Ramamoorthy, A. (2012). Does cholesterol play a
636 role in the bacterial selectivity of antimicrobial peptides? Front Immunol *3*, 195.
637 Brogden, K.A. (2005). Antimicrobial peptides: pore formers or metabolic
638 inhibitors in bacteria? Nat Rev Microbiol *3*, 238-250.
639 Bullard, R.S., Gibson, W., Bose, S.K., Belgrave, J.K., Eaddy, A.C., Wright, C.J., Hazen-
640 Martin, D.J., Lage, J.M., Keane, T.E., Ganz, T.A.*, et al.* (2008). Functional analysis of
641 the host defense peptide Human Beta Defensin-1: new insight into its potential
642 role in cancer. Mol Immunol *45*, 839-848.
643 Bunker, B.D., Nellimoottil, T.T., Boileau, R.M., Classen, A.K., and Bilder, D. (2015).
644 The transcriptional response to tumorigenic polarity loss in Drosophila. Elife *4*.
645 Cao, J., Ni, J., Ma, W., Shiu, V., Milla, L.A., Park, S., Spletter, M.L., Tang, S., Zhang, J.,
646 Wei, X.*, et al.* (2014). Insight into insulin secretion from transcriptome and
647 genetic analysis of insulin-producing cells of Drosophila. Genetics *197*, 175-192.
648 Cao, Y., Chtarbanova, S., Petersen, A.J., and Ganetzky, B. (2013). Dnr1 mutations
649 cause neurodegeneration in Drosophila by activating the innate immune
650 response in the brain. Proc Natl Acad Sci U S A *110*, E1752-1760.
651 Chung, E.M.C., Dean, S.N., Propst, C.N., Bishop, B.M., and van Hoek, M.L. (2017).
652 Komodo dragon-inspired synthetic peptide DRGN-1 promotes wound-healing of
653 a mixed-biofilm infected wound. NPJ Biofilms Microbiomes *3*, 9.
654 Cordero, J.B., Macagno, J.P., Stefanatos, R.K., Strathdee, K.E., Cagan, R.L., and Vidal,
655 M. (2010). Oncogenic Ras diverts a host TNF tumor suppressor activity into
656 tumor promoter. Dev Cell *18*, 999-1011.
657 Deslouches, B., and Di, Y.P. (2017). Antimicrobial peptides with selective
658 antitumor mechanisms: prospect for anticancer applications. Oncotarget.
659 Donald, C.D., Sun, C.Q., Lim, S.D., Macoska, J., Cohen, C., Amin, M.B., Young, A.N.,
660 Ganz, T.A., Marshall, F.F., and Petros, J.A. (2003). Cancer-specific loss of beta-
661 defensin 1 in renal and prostatic carcinomas. Lab Invest *83*, 501-505.
662 Fernandez-Ayala, D.J., Sanz, A., Vartiainen, S., Kemppainen, K.K., Babusiak, M.,
663 Mustalahti, E., Costa, R., Tuomela, T., Zeviani, M., Chung, J.*, et al.* (2009).
664 Expression of the Ciona intestinalis alternative oxidase (AOX) in Drosophila
665 complements defects in mitochondrial oxidative phosphorylation. Cell Metab *9*,
666 449-460.

667 Fogarty, C.E., Diwanji, N., Lindblad, J.L., Tare, M., Amcheslavsky, A., Makhijani, K.,
668 Bruckner, K., Fan, Y., and Bergmann, A. (2016). Extracellular Reactive Oxygen
669 Species Drive Apoptosis-Induced Proliferation via Drosophila Macrophages. Curr
670 Biol *26*, 575-584.
671 Ham, B., Fernandez, M.C., D'Costa, Z., and Brodt, P. (2016). The diverse roles of
672 the TNF axis in cancer progression and metastasis. Trends Cancer Res *11*, 1-27.
673 Hanson, M.A., Dostalova, A., Ceroni, C., Poidevin, M., Kondo, S., and Lemaitre, B.
674 (2018). Synergy and remarkable specificity of antimicrobial peptides in vivo
675 using a systematic knockout approach. BioRxiv.
676 Hoffmann, J.A., and Reichhart, J.M. (2002). Drosophila innate immunity: an
677 evolutionary perspective. Nat Immunol *3*, 121-126.
678 Hollingsworth, M.A., and Swanson, B.J. (2004). Mucins in cancer: protection and
679 control of the cell surface. Nat Rev Cancer *4*, 45-60.
680 Igaki, T., Kanda, H., Yamamoto-Goto, Y., Kanuka, H., Kuranaga, E., Aigaki, T., and
681 Miura, M. (2002). Eiger, a TNF superfamily ligand that triggers the Drosophila
682 JNK pathway. EMBO J *21*, 3009-3018.
683 Igaki, T., Pagliarini, R.A., and Xu, T. (2006). Loss of cell polarity drives tumor
684 growth and invasion through JNK activation in Drosophila. Curr Biol *16*, 1139-
685 1146.
686 Igaki, T., Pastor-Pareja, J.C., Aonuma, H., Miura, M., and Xu, T. (2009). Intrinsic
687 tumor suppression and epithelial maintenance by endocytic activation of
688 Eiger/TNF signaling in Drosophila. Dev Cell *16*, 458-465.
689 Imler, J.L., and Zheng, L. (2004). Biology of Toll receptors: lessons from insects
690 and mammals. J Leukoc Biol *75*, 18-26.
691 Iwasaki, T., Ishibashi, J., Tanaka, H., Sato, M., Asaoka, A., Taylor, D., and
692 Yamakawa, M. (2009). Selective cancer cell cytotoxicity of enantiomeric 9-mer
693 peptides derived from beetle defensins depends on negatively charged
694 phosphatidylserine on the cell surface. Peptides *30*, 660-668.
695 Ji, S., Sun, M., Zheng, X., Li, L., Sun, L., Chen, D., and Sun, Q. (2014). Cell-surface
696 localization of Pellino antagonizes Toll-mediated innate immune signalling by
697 controlling MyD88 turnover in Drosophila. Nat Commun *5*, 3458.
698 Knelson, E.H., Nee, J.C., and Blobe, G.C. (2014). Heparan sulfate signaling in
699 cancer. Trends Biochem Sci *39*, 277-288.
700 Kounatidis, I., Chtarbanova, S., Cao, Y., Hayne, M., Jayanth, D., Ganetzky, B., and
701 Ligoxygakis, P. (2017). NF-kappaB Immunity in the Brain Determines Fly
702 Lifespan in Healthy Aging and Age-Related Neurodegeneration. Cell Rep *19*, 836-
703 848.
704 Kulshammer, E., Mundorf, J., Kilinc, M., Frommolt, P., Wagle, P., and Uhlirova, M.
705 (2015). Interplay among Drosophila transcription factors Ets21c, Fos and Ftz-F1
706 drives JNK-mediated tumor malignancy. Dis Model Mech *8*, 1279-1293.
707 Lemaitre, B., Nicolas, E., Michaut, L., Reichhart, J.M., and Hoffmann, J.A. (1996).
708 The dorsoventral regulatory gene cassette spatzle/Toll/cactus controls the
709 potent antifungal response in Drosophila adults. Cell *86*, 973-983.
710 Leulier, F., Rodriguez, A., Khush, R.S., Abrams, J.M., and Lemaitre, B. (2000). The
711 Drosophila caspase Dredd is required to resist gram-negative bacterial infection.
712 EMBO Rep *1*, 353-358.
713 Levashina, E.A., Ohresser, S., Bulet, P., Reichhart, J.M., Hetru, C., and Hoffmann, J.A.
714 (1995). Metchnikowin, a novel immune-inducible proline-rich peptide from

715 Drosophila with antibacterial and antifungal properties. Eur J Biochem *233*, 694-
716 700.
717 Lezi, E., Zhou, T., Koh, S., Chuang, M., Sharma, R., Pujol, N., Chisholm, A.D., Eroglu,
718 C., Matsunami, H., and Yan, D. (2018). An Antimicrobial Peptide and Its Neuronal
719 Receptor Regulate Dendrite Degeneration in Aging and Infection. Neuron *97*,
720 125-138 e125.
721 Mergaert, P., Kikuchi, Y., Shigenobu, S., and Nowack, E.C.M. (2017). Metabolic
722 Integration of Bacterial Endosymbionts through Antimicrobial Peptides. Trends
723 Microbiol *25*, 703-712.
724 Moreno, E., Yan, M., and Basler, K. (2002). Evolution of TNF signaling
725 mechanisms: JNK-dependent apoptosis triggered by Eiger, the Drosophila
726 homolog of the TNF superfamily. Curr Biol *12*, 1263-1268.
727 Parameswaran, N., and Patial, S. (2010). Tumor Necrosis Factor-α Signaling in
728 Macrophages. Crit Rev Eukaryot Gene Expr *20*, 87-103.
729 Parisi, F., Stefanatos, R.K., Strathdee, K., Yu, Y., and Vidal, M. (2014). Transformed
730 epithelia trigger non-tissue-autonomous tumor suppressor response by
731 adipocytes via activation of Toll and Eiger/TNF signaling. Cell Rep *6*, 855-867.
732 Parvy, J.P., Hodgson, J.A., and Cordero, J.B. (2018). Drosophila as a Model System
733 to Study Nonautonomous Mechanisms Affecting Tumour Growth and Cell Death.
734 Biomed Res Int *2018*, 7152962.
735 Pastor-Pareja, J.C., Grawe, F., Martin-Blanco, E., and Garcia-Bellido, A. (2004).
736 Invasive cell behavior during Drosophila imaginal disc eversion is mediated by
737 the JNK signaling cascade. Dev Cell *7*, 387-399.
738 Riedl, S., Rinner, B., Asslaber, M., Schaider, H., Walzer, S., Novak, A., Lohner, K.,
739 and Zweytick, D. (2011). In search of a novel target - phosphatidylserine exposed
740 by non-apoptotic tumor cells and metastases of malignancies with poor
741 treatment efficacy. Biochim Biophys Acta *1808*, 2638-2645.
742 Santabarbara-Ruiz, P., Lopez-Santillan, M., Martinez-Rodriguez, I., Binagui-Casas,
743 A., Perez, L., Milan, M., Corominas, M., and Serras, F. (2015). ROS-Induced JNK
744 and p38 Signaling Is Required for Unpaired Cytokine Activation during
745 Drosophila Regeneration. PLoS Genet *11*, e1005595.
746 Shafee, T.M., Lay, F.T., Phan, T.K., Anderson, M.A., and Hulett, M.D. (2017).
747 Convergent evolution of defensin sequence, structure and function. Cell Mol Life
748 Sci *74*, 663-682.
749 Shklyar, B., Levy-Adam, F., Mishnaevski, K., and Kurant, E. (2013). Caspase
750 activity is required for engulfment of apoptotic cells. Mol Cell Biol *33*, 3191-3201.
751 Srivastava, A., Pastor-Pareja, J.C., Igaki, T., Pagliarini, R., and Xu, T. (2007).
752 Basement membrane remodeling is essential for Drosophila disc eversion and
753 tumor invasion. Proc Natl Acad Sci U S A *104*, 2721-2726.
754 Sun, C.Q., Arnold, R., Fernandez-Golarz, C., Parrish, A.B., Almekinder, T., He, J., Ho,
755 S.M., Svoboda, P., Pohl, J., Marshall, F.F.*, et al.* (2006). Human beta-defensin-1, a
756 potential chromosome 8p tumor suppressor: control of transcription and
757 induction of apoptosis in renal cell carcinoma. Cancer Res *66*, 8542-8549.
758 Teng, M.W., Swann, J.B., Koebel, C.M., Schreiber, R.D., and Smyth, M.J. (2008).
759 Immune-mediated dormancy: an equilibrium with cancer. J Leukoc Biol *84*, 988-
760 993.
761 Tjabringa, G.S., Aarbiou, J., Ninaber, D.K., Drijfhout, J.W., Sorensen, O.E.,
762 Borregaard, N., Rabe, K.F., and Hiemstra, P.S. (2003). The antimicrobial peptide
763 LL-37 activates innate immunity at the airway epithelial surface by

764 transactivation of the epidermal growth factor receptor. J Immunol *171*, 6690-
765 6696.
766 Tokumaru, S., Sayama, K., Shirakata, Y., Komatsuzawa, H., Ouhara, K., Hanakawa,
767 Y., Yahata, Y., Dai, X., Tohyama, M., Nagai, H., *et al.* (2005). Induction of
768 keratinocyte migration via transactivation of the epidermal growth factor
769 receptor by the antimicrobial peptide LL-37. J Immunol *175*, 4662-4668.
770 Tung, T.T., Nagaosa, K., Fujita, Y., Kita, A., Mori, H., Okada, R., Nonaka, S., and
771 Nakanishi, Y. (2013). Phosphatidylserine recognition and induction of apoptotic
772 cell clearance by Drosophila engulfment receptor Draper. J Biochem *153*, 483-
773 491.
774 Tzou, P., De Gregorio, E., and Lemaitre, B. (2002). How Drosophila combats
775 microbial infection: a model to study innate immunity and host-pathogen
776 interactions. Curr Opin Microbiol *5*, 102-110.
777 Tzou, P., Ohresser, S., Ferrandon, D., Capovilla, M., Reichhart, J.M., Lemaitre, B.,
778 Hoffmann, J.A., and Imler, J.L. (2000). Tissue-specific inducible expression of
779 antimicrobial peptide genes in Drosophila surface epithelia. Immunity *13*, 737-
780 748.
781 Uhlirova, M., and Bohmann, D. (2006). JNK- and Fos-regulated Mmp1 expression
782 cooperates with Ras to induce invasive tumors in Drosophila. EMBO J *25*, 5294-
783 5304.
784 van Wetering, S., Mannesse-Lazeroms, S.P., van Sterkenburg, M.A., and Hiemstra,
785 P.S. (2002). Neutrophil defensins stimulate the release of cytokines by airway
786 epithelial cells: modulation by dexamethasone. Inflamm Res *51*, 8-15.
787 Wang, C., Chen, Y.W., Zhang, L., Gong, X.G., Zhou, Y., and Shang, D.J. (2016).
788 Melanoma cell surface-expressed phosphatidylserine as a therapeutic target for
789 cationic anticancer peptide, temporin-1CEa. J Drug Target *24*, 548-556.
790 Wang, C., Dong, S., Zhang, L., Zhao, Y., Huang, L., Gong, X., Wang, H., and Shang, D.
791 (2017). Cell surface binding, uptaking and anticancer activity of L-K6, a
792 lysine/leucine-rich peptide, on human breast cancer MCF-7 cells. Sci Rep *7*, 8293.
793 Wilson, C.L., Ouellette, A.J., Satchell, D.P., Ayabe, T., Lopez-Boado, Y.S., Stratman,
794 J.L., Hultgren, S.J., Matrisian, L.M., and Parks, W.C. (1999). Regulation of intestinal
795 alpha-defensin activation by the metalloproteinase matrilysin in innate host
796 defense. Science *286*, 113-117.
797 Wilson, C.L., Schmidt, A.P., Pirila, E., Valore, E.V., Ferri, N., Sorsa, T., Ganz, T., and
798 Parks, W.C. (2009). Differential Processing of {alpha}- and {beta}-Defensin
799 Precursors by Matrix Metalloproteinase-7 (MMP-7). J Biol Chem *284*, 8301-8311.
800 Ye, Z., Dong, H., Li, Y., Ma, T., Huang, H., Leong, H.S., Eckel-Passow, J., Kocher, J.A.,
801 Liang, H., and Wang, L. (2018). Prevalent Homozygous Deletions of Type I
802 Interferon and Defensin Genes in Human Cancers Associate with
803 Immunotherapy Resistance. Clin Cancer Res *24*, 3299-3308.
804 Yeaman, M.R., and Yount, N.Y. (2003). Mechanisms of antimicrobial peptide
805 action and resistance. Pharmacol Rev *55*, 27-55.
806 Zhao, H.W., Zhou, D., and Haddad, G.G. (2011). Antimicrobial peptides increase
807 tolerance to oxidant stress in Drosophila melanogaster. J Biol Chem *286*, 6211-
808 6218.
809 Zhu, M., Xin, T., Weng, S., Gao, Y., Zhang, Y., Li, Q., and Li, M. (2010). Activation of
810 JNK signaling links lgl mutations to disruption of the cell polarity and epithelial
811 organization in Drosophila imaginal discs. Cell Res *20*, 242-245.
812

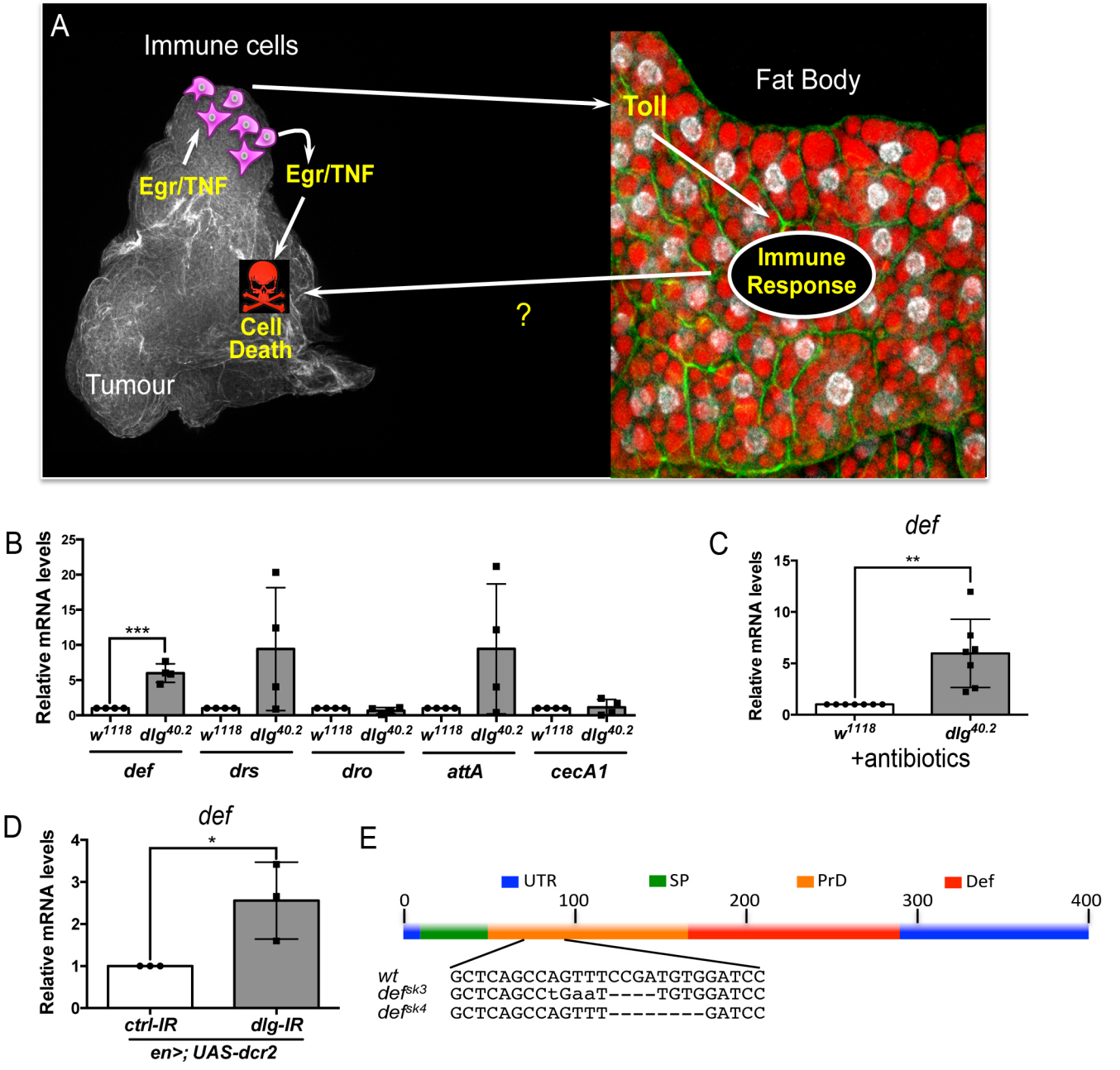
A
Immune cells
Egr/TNF
Egr/TNF
Cell Death
Tumour
Fat Body
Toll
Immune Response
?
B
Relative mRNA levels
***
w1118
dlg40.2
def
drs
dro
attA
cecA1
C
def
**
+antibiotics
D
def
*
ctrl-IR
dlg-IR
en>; UAS-dcr2
E
UTR
SP
PrD
Def
0
100
200
300
400
wt GCTCAGCCAGTTTCCGATGTGGATCC
defsk3 GCTCAGCCtGaaT----TGTGGATCC
defsk4 GCTCAGCCAGTTT--------GATCC

Figure 1

Figure Legends

Figure 1 | *def* is induced in *dlg* mutant tumour bearing animals. A, Working model showing the cooperation between haemocyte-derived TNF and the immune response in the fat body in tumour cell death (Parisi et al, 2014). B, RT-qPCR analyses showing expression of several AMPs in the fat body of $dlg^{40.2}$ mutant tumour bearing larvae compared to wild-type (w^{1118}) larvae (n=4). C, RT-qPCR analysis of *def* expression in w^{1118} and $dlg^{40.2}$ whole larvae reared on antibiotics (n=7). D, RT-qPCR analysis showing *def* expression in larvae expressing a *ctrl-IR* or a *dlg-IR* in the posterior part of the wing disc (*en>;UAS-dcr2*) (n=3). E, Schematic representation of the *def* gene locus showing mutant alleles generated (UTR: Untranslated Regions, SP: Signal Peptide, PrD: Pro-Domain, Def: Mature Defensin). Statistical analysis: B-D, Student t-test, B, ***p=0.0003, C, **p=0.0074, D, *p=0.042.

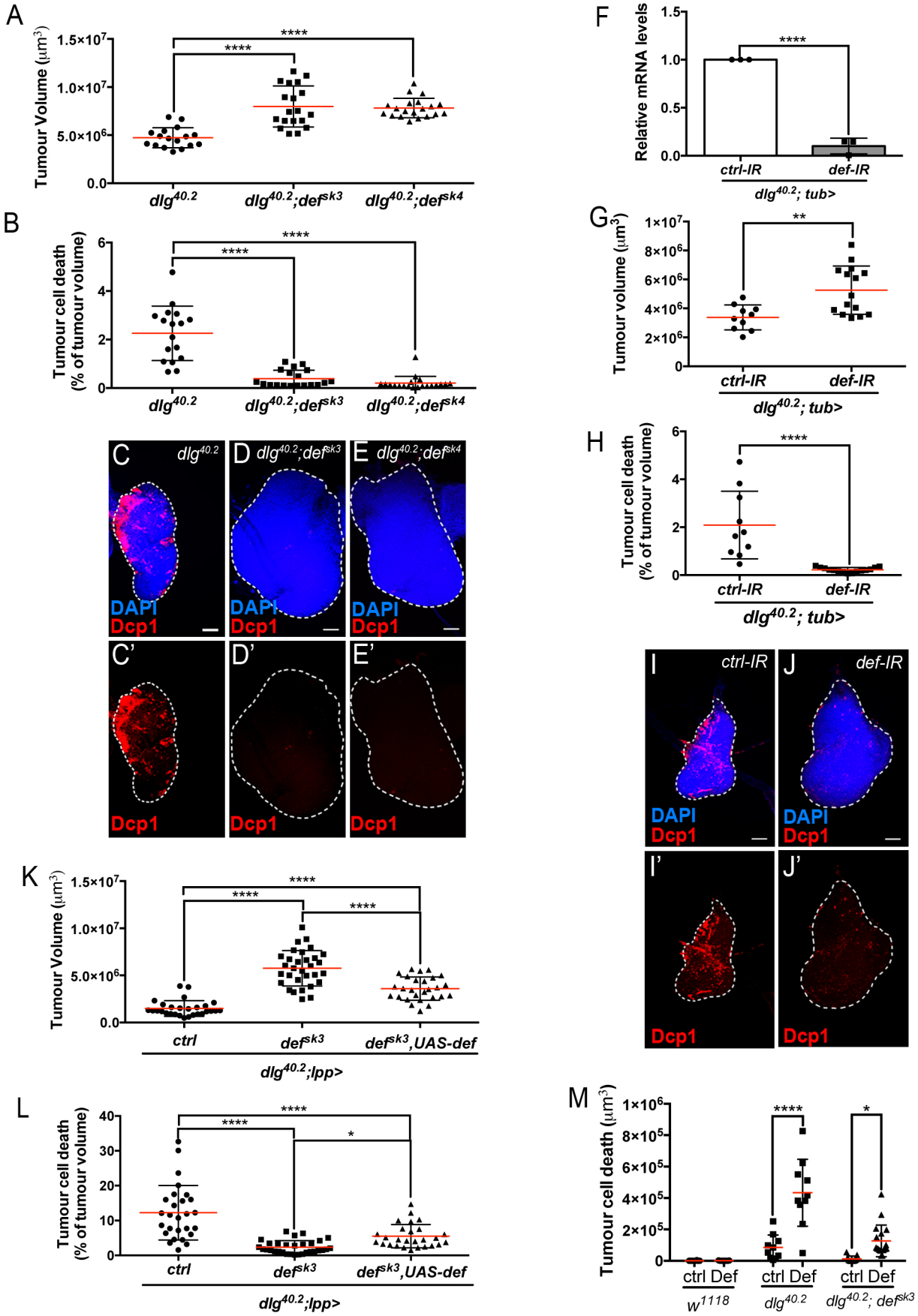
A
Tumour Volume (μm³)
1.5×10⁷
1.0×10⁷
5.0×10⁶
0.0
****
****
dlg40.2
dlg40.2;defsk3
dlg40.2;defsk4
B
Tumour cell death (% of tumour volume)
6
4
2
0
****
****
dlg40.2
dlg40.2;defsk3
dlg40.2;defsk4
C
dlg40.2
D
dlg40.2;defsk3
E
dlg40.2;defsk4
DAPI
Dcp1
C'
D'
E'
Dcp1
F
Relative mRNA levels
1.5
1.0
0.5
0.0
****
ctrl-IR
def-IR
dlg40.2; tub>
G
Tumour volume (μm³)
1×10⁷
8×10⁶
6×10⁶
4×10⁶
2×10⁶
0
**
ctrl-IR
def-IR
dlg40.2; tub>
H
Tumour cell death (% of tumour volume)
6
4
2
0
****
ctrl-IR
def-IR
dlg40.2; tub>
I
ctrl-IR
J
def-IR
DAPI
Dcp1
I'
J'
Dcp1
K
Tumour Volume (μm³)
1.5×10⁷
1.0×10⁷
5.0×10⁶
0.0
****
****
****
ctrl
defsk3
defsk3,UAS-def
dlg40.2;lpp>
L
Tumour cell death (% of tumour volume)
40
30
20
10
0
****
****
*
ctrl
defsk3
defsk3,UAS-def
dlg40.2;lpp>
M
Tumour cell death (μm³)
1×10⁶
8×10⁵
6×10⁵
4×10⁵
2×10⁵
0
****
*
ctrl Def
ctrl Def
ctrl Def
w1118
dlg40.2
dlg40.2; defsk3

Figure 2

Figure 2 | Def restricts tumour growth and promotes tumour cell death.
A-E', Quantification of tumour volume (TV) (A) and tumour cell death (TCD) (B) in wing imaginal discs from *dlg*$^{40.2}$ (n=17), *dlg*$^{40.2}$*;def*^{sk3} (n=19) and *dlg*$^{40.2}$*;def*^{sk4} (n=20) mutant larvae and representative immunofluorescence images of tissues quantified (C-E'). F, RT-qPCR analysis showing *def* expression upon ubiquitous knockdown (*dlg*$^{40.2}$*;tub>*) (n=3). G-J', Quantification of TV (G) and TCD (H) in wing imaginal discs from larvae ubiquitously expressing a *control-IR* (*ctrl-IR*: n=10) or a *def-IR* (n=15) and representative immunofluorescence images of tissues quantified (I-J'). K-L, Quantification of TV (G) and TCD (H) in wing imaginal discs from *dlg* mutant controls (*dlg*$^{40.2}$*;lpp>*: n=28), *dlg;def*^{sk3} mutants controls (*dlg*$^{40.2}$*;def*^{sk3}*;lpp>*: n=31) or *dlg;def*^{sk3} mutants expressing *def* in the fat body (*dlg*$^{40.2}$*;def*^{sk3}*,UAS-def;lpp>*: n=27). M, Effect of PBS (ctrl) or synthetic Def injection on TCD from wild-type larvae (*w*^{1118}, ctrl: n=10, Def: n=9), *dlg*$^{40.2}$ (ctrl: n=10, Def: n=10) and *dlg*$^{40.2}$*;def*^{sk3} (ctrl: n=11, Def: n=18) mutant larvae. Tissues were stained with 4',6-diamidino-2-phenylindole (DAPI, blue) for nuclei visualization and with anti-cleaved Decapping protein 1 (Dcp1) antibody (red) to detect apoptotic cell death. Scale bars=50 µm. <u>Statistical analysis:</u> A, B, K, N, One way ANOVA, *p<0.05, ****p<0.0001; F, Student t-test, ****p<0.0001, G-H, Mann-Whitney test, G, **p=0.0054, H, ****p<0.0001; M, Two way ANOVA (only relevant significant statistics are indicated), *p<0.05, ****p<0.0001.

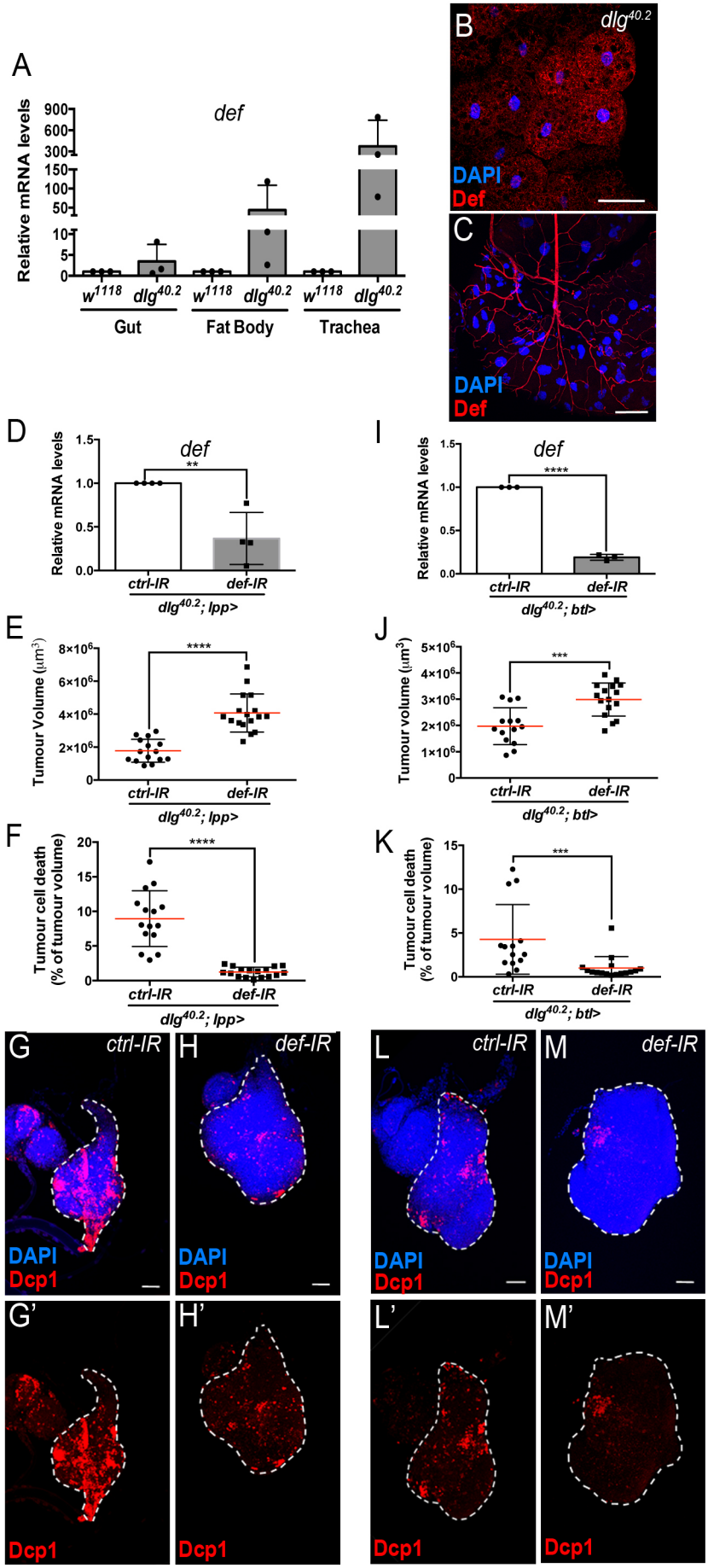
A
def
Relative mRNA levels
900
600
300
150
100
50
10
5
0
w1118
dlg40.2
Gut
Fat Body
Trachea
B
dlg40.2
DAPI
Def
C
DAPI
Def
D
def
Relative mRNA levels
1.5
1.0
0.5
0.0
**
ctrl-IR
def-IR
dlg40.2; lpp>
E
Tumour Volume (μm3)
8×106
6×106
4×106
2×106
0
****
ctrl-IR
def-IR
dlg40.2; lpp>
F
Tumour cell death (% of tumour volume)
20
15
10
5
0
****
ctrl-IR
def-IR
dlg40.2; lpp>
I
def
Relative mRNA levels
1.5
1.0
0.5
0.0
****
ctrl-IR
def-IR
dlg40.2; btl>
J
Tumour volume (μm3)
5×106
4×106
3×106
2×106
1×106
0
***
ctrl-IR
def-IR
dlg40.2; btl>
K
Tumour cell death (% of tumour volume)
15
10
5
0
***
ctrl-IR
def-IR
dlg40.2; btl>
G
ctrl-IR
DAPI
Dcp1
H
def-IR
DAPI
Dcp1
L
ctrl-IR
DAPI
Dcp1
M
def-IR
DAPI
Dcp1
G'
Dcp1
H'
Dcp1
L'
Dcp1
M'
Dcp1

Figure 3

Figure 3 | Def from the trachea and the fat body mediates tumour cell death. A, RT-qPCR analysis of *def* expression in gut, fat body and trachea dissected from w^{1118} or $dlg^{40.2}$ mutant larvae (n=3). B-C, Fat body (B) and trachea (C) from $dlg^{40.2}$ mutant larvae stained with DAPI (blue) and anti-Def antibody (red). D, RT-qPCR analysis of *def* expression from $dlg^{40.2}$ mutant larvae ($dlg^{40.2}$*;lpp>*) expressing a *ctrl-IR* or *def-IR* in the fat body (n=4). E-H', Quantification of TV (E) and TCD (F) in wing imaginal discs from $dlg^{40.2}$ mutant larvae ($dlg^{40.2}$*;lpp>*) expressing a *ctrl-IR* (n=15) or *def-IR* (n=17) in the fat body and representative immunofluorescence images of tissues quantified (G-H'). I, RT-qPCR analysis of *def* expression from $dlg^{40.2}$ mutant larvae ($dlg^{40.2}$*;btl>*) expressing a *ctrl-IR* or *def-IR* in the trachea (n=3). J-M', Quantification of TV (J) and TCD (K) in wing imaginal discs from $dlg^{40.2}$ mutant larvae ($dlg^{40.2}$*;btl>*) expressing a *ctrl-IR* (n=14) or *def-IR* (n=16) in the trachea and representative immunofluorescence images of tissues quantified (L-M'). Tumours were stained with DAPI (blue) and anti-Dcp1 antibody (red). Scale bars=50 µm. Statistical analysis: A, D, I, Student t-test, D, **p=0.0054, I, ****p<0.0001; E, F, J, K, Mann-Whitney test, E, F, ****p<0.0001, J, ***p=0.0009, K, ***p=0.0004.

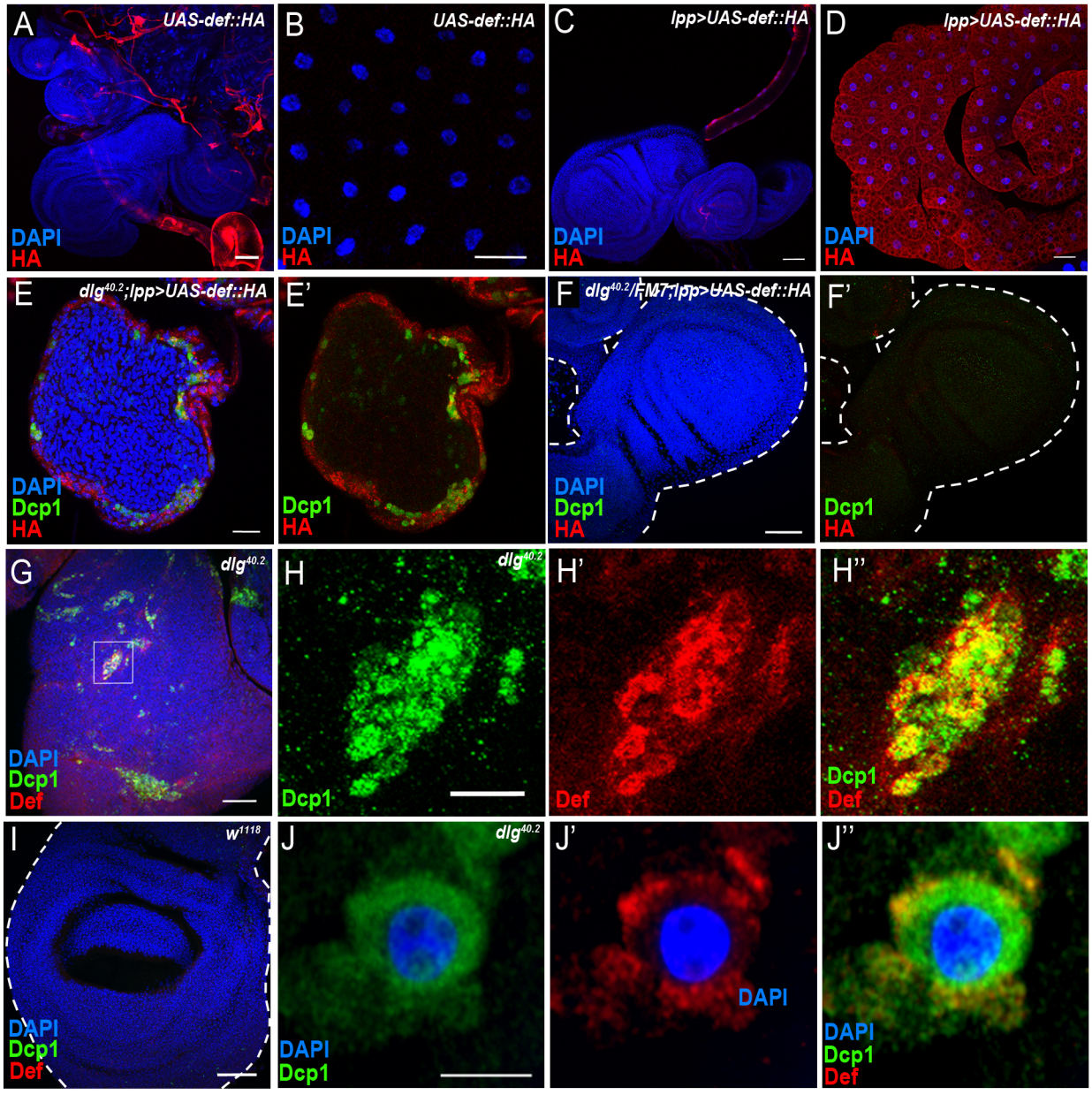
A
UAS-def::HA
DAPI
HA
B
UAS-def::HA
DAPI
HA
C
lpp>UAS-def::HA
DAPI
HA
D
lpp>UAS-def::HA
DAPI
HA
E
dlg40.2;lpp>UAS-def::HA
DAPI
Dcp1
HA
E'
Dcp1
HA
F
dlg40.2/FM7;lpp>UAS-def::HA
DAPI
Dcp1
HA
F'
Dcp1
HA
G
dlg40.2
DAPI
Dcp1
Def
H
dlg40.2
Dcp1
H'
Def
H''
Dcp1
Def
I
w1118
DAPI
Dcp1
Def
J
dlg40.2
DAPI
Dcp1
J'
DAPI
J''
DAPI
Dcp1
Def

Figure 4

Figure 4 | Def produced by immune tissues specifically targets tumour cells. A-B, DAPI (blue) and anti-HA antibody (red) staining showing expression of def-HA construct in trachea (A) but not in fat body (B) of *UAS-def-HA* larvae. C-D, DAPI (blue) and anti-HA antibody (red) staining showing expression of a *UAS-def-HA* transgene in the fat body and the trachea when driven by a fat body specific driver (*lpp>UAS-def-HA*). E-E', DAPI (white), anti-Dcp1 (green) and anti-HA antibody (red) staining of $dlg^{40.2}$ mutant tumour from larvae expressing the *def-HA* construct in the fat body and the trachea ($dlg^{40.2}$*;lpp>UAS-def-HA*). F-F', DAPI (white), anti-Dcp1 (green) and anti-HA antibody (red) staining of $dlg^{40.2}$ heterozygous wing disc from larvae expressing the *def-HA* construct in the fat body ($dlg^{40.2}$*/FM7;lpp>UAS-def-HA*). G-H'', $dlg^{40.2}$ mutant tumour stained with DAPI (blue), anti-Def (red) and anti-Dcp1 (green) antibodies. I, wild type (w^{1118}) wing imaginal disc stained with DAPI (blue), anti-Def (red) and anti-Dcp1 (green) antibodies. J-J'', High-resolution imaging of a single dying tumour cell stained with DAPI (blue), anti-Def (red) and anti-Dcp1 (green) antibodies. A-I, Scale bars=50 μm, J-J'', Scale bar=2.5 μm.

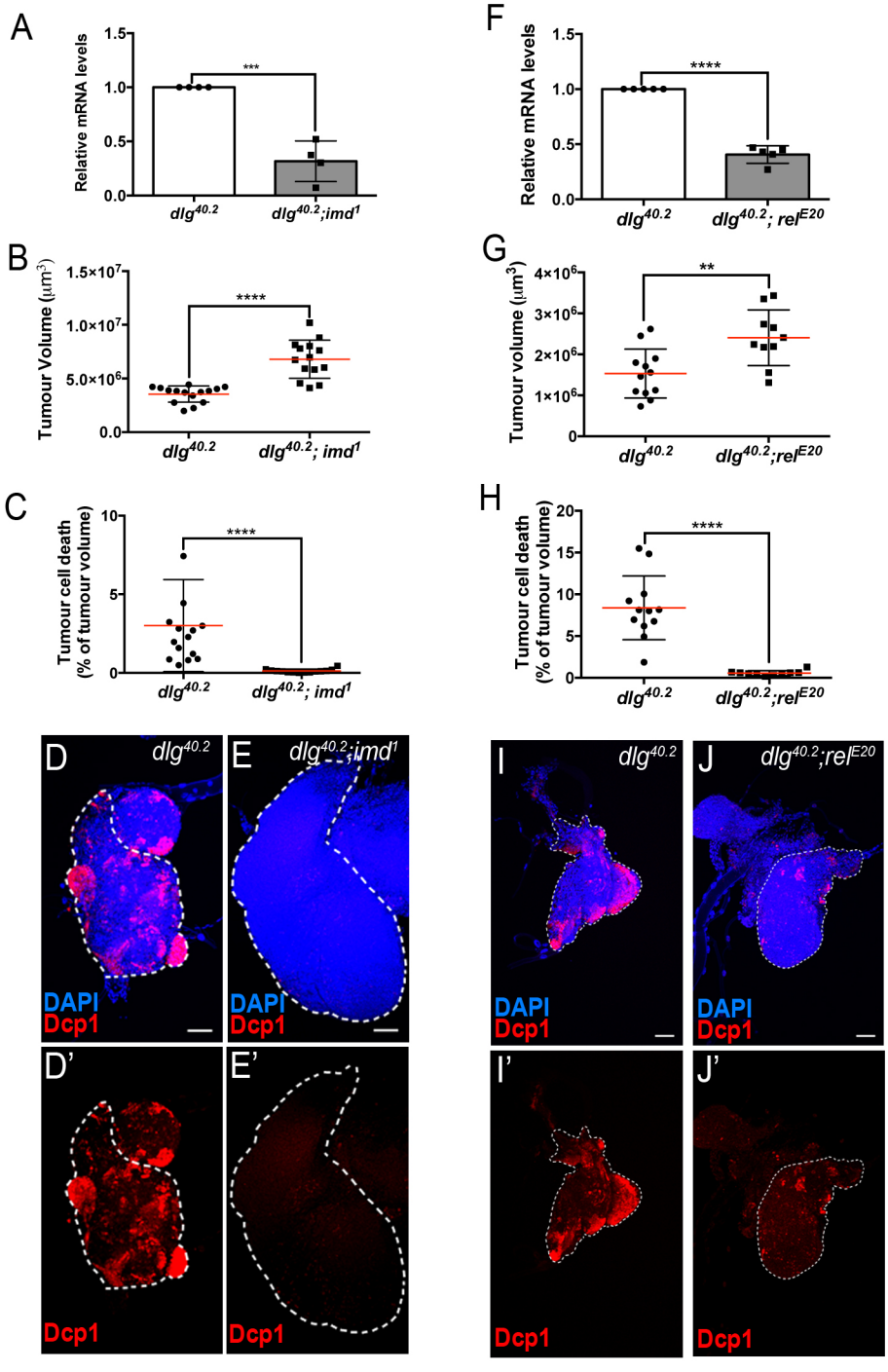
A
Relative mRNA levels
1.5
1.0
0.5
0.0
***
dlg40.2
dlg40.2;imd1
B
Tumour Volume (µm3)
1.5×107
1.0×107
5.0×106
0.0
****
dlg40.2
dlg40.2; imd1
C
Tumour cell death (% of tumour volume)
10
5
0
****
dlg40.2
dlg40.2; imd1
F
Relative mRNA levels
1.5
1.0
0.5
0.0
****
dlg40.2
dlg40.2; relE20
G
Tumour volume (µm3)
4×106
3×106
2×106
1×106
0
**
dlg40.2
dlg40.2;relE20
H
Tumour cell death (% of tumour volume)
20
15
10
5
0
****
dlg40.2
dlg40.2;relE20
D
dlg40.2
DAPI
Dcp1
E
dlg40.2;imd1
DAPI
Dcp1
D'
Dcp1
E'
Dcp1
I
dlg40.2
DAPI
Dcp1
J
dlg40.2;relE20
DAPI
Dcp1
I'
Dcp1
J'
Dcp1

Figure 5

Figure 5 | Imd pathway activation is required for *def* expression and Def-mediated tumour cell death. A, RT-qPCR analysis of *def* expression from $dlg^{40.2}$ and $dlg^{40.2}$;imd^{1} mutant larvae (n=4). B-E', Quantification of TV (B) and TCD (C) in wing imaginal discs from $dlg^{40.2}$ (n=15) and $dlg^{40.2}$;imd^{1} (n=14) mutants larvae and representative immunofluorescence images of tissues quantified stained with DAPI (blue) and anti-Dcp1 antibody (red) (D-E'). F, RT-qPCR analysis showing *def* expression in $dlg^{40.2}$ and $dlg^{40.2}$; rel^{E20} mutant animals (n=5). G-J', Quantification of TV (G) and TCD (H) from $dlg^{40.2}$ (n=12) and $dlg^{40.2}$;rel^{E20} (n=10) mutant larvae and representative pictures of the corresponding tumours (I-J'). Scale bars=50 µm. Statistical analysis: A, F, Student t-test, A, ***p<0.0003, F, ****p<0.0001; B, C, G, H, Mann-Whitney test, B, C, H, ****p<0.0001, G, **p=0.009.

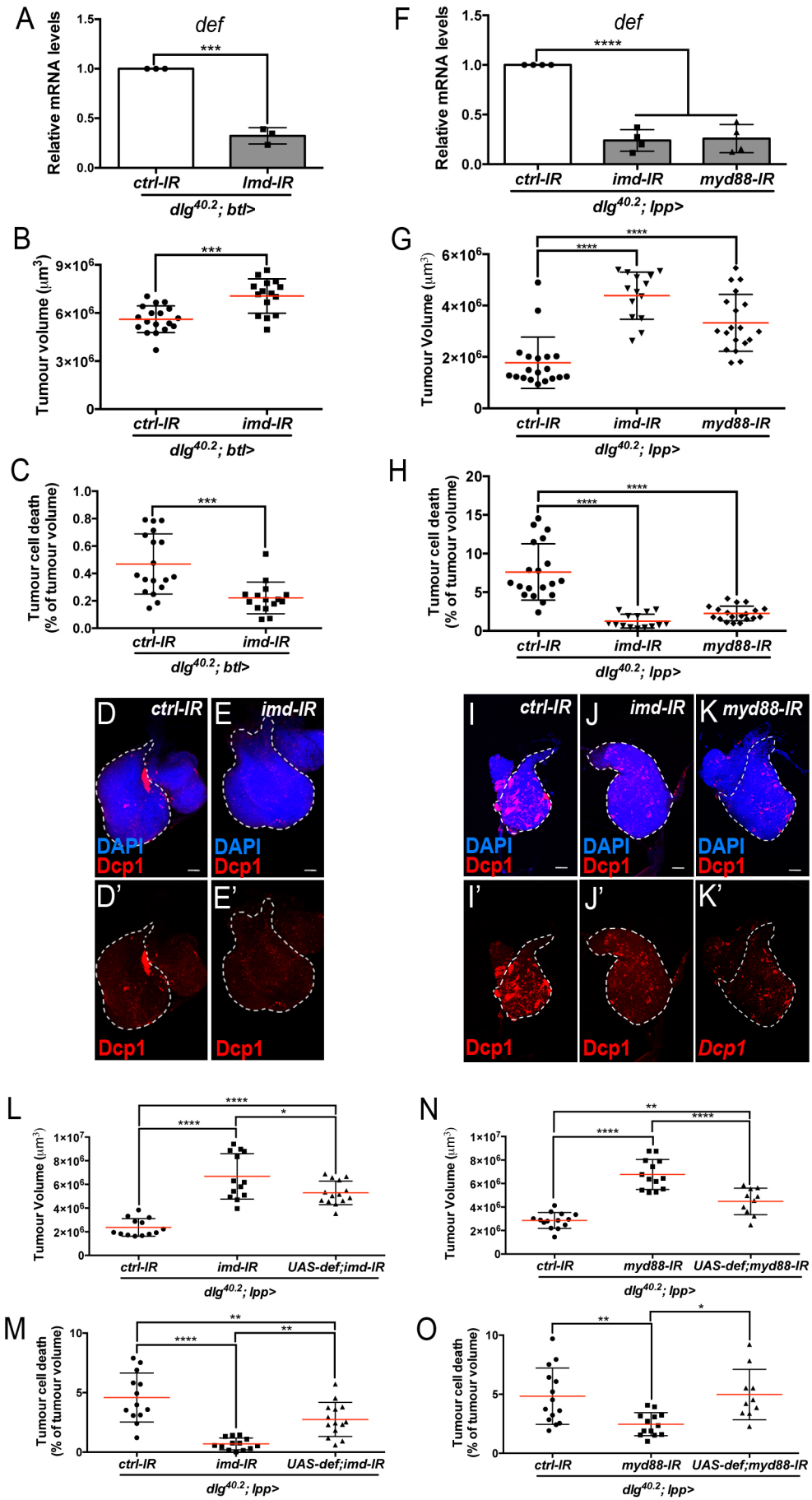
A
def
Relative mRNA levels
1.5
1.0
0.5
0.0
***
ctrl-IR
Imd-IR
dlg40.2; btl>
B
Tumour volume (µm3)
9×106
6×106
3×106
0
***
ctrl-IR
imd-IR
dlg40.2; btl>
C
Tumour cell death (% of tumour volume)
1.0
0.8
0.6
0.4
0.2
0.0
***
ctrl-IR
imd-IR
dlg40.2; btl>
F
def
Relative mRNA levels
1.5
1.0
0.5
0.0
****
ctrl-IR
imd-IR
myd88-IR
dlg40.2; lpp>
G
Tumour Volume (µm3)
6×106
4×106
2×106
0
****
****
ctrl-IR
imd-IR
myd88-IR
dlg40.2; lpp>
H
Tumour cell death (% of tumour volume)
20
15
10
5
0
****
****
ctrl-IR
imd-IR
myd88-IR
dlg40.2; lpp>
D ctrl-IR
E imd-IR
DAPI
Dcp1
D'
E'
Dcp1
I ctrl-IR
J imd-IR
K myd88-IR
DAPI
Dcp1
I'
J'
K'
Dcp1
L
Tumour Volume (µm3)
1×107
8×106
6×106
4×106
2×106
0
****
****
*
ctrl-IR
imd-IR
UAS-def;imd-IR
dlg40.2; lpp>
N
Tumour Volume (µm3)
1×107
8×106
6×106
4×106
2×106
0
**
****
****
ctrl-IR
myd88-IR
UAS-def;myd88-IR
dlg40.2; lpp>
M
Tumour cell death (% of tumour volume)
10
5
0
**
****
**
ctrl-IR
imd-IR
UAS-def;imd-IR
dlg40.2; lpp>
O
Tumour cell death (% of tumour volume)
10
5
0
**
*
ctrl-IR
myd88-IR
UAS-def;myd88-IR
dlg40.2; lpp>

Figure 6

Figure 6 | Imd and Toll pathway activation are required in the trachea and the fat body to promote Defensin-dependent tumour cell death. A, RT-qPCR analysis of *def* expression from *dlg*$^{40.2}$ mutant larvae (*dlg*$^{40.2}$*;btl>*) expressing a *ctrl-IR* or *imd-IR* in the trachea (n=3). B-E', Quantification of TV (B) and TCD (C) from *dlg*$^{40.2}$ mutant larvae (*dlg*$^{40.2}$*;btl>*) expressing a *ctrl-IR* (n=18) or *imd-IR* (n=15) in the trachea and representative immunofluorescence images of tissues quantified stained with DAPI (blue) and anti-Dcp1 antibody (red) (D-E'). F, RT-qPCR analysis of *def* expression from *dlg*$^{40.2}$ mutant larvae (*dlg*$^{40.2}$*;lpp>*) expressing a *ctrl-IR*, an *imd-IR* or a myd88-IR in the fat body. G-K', Quantification of TV (G) and TCD (H) from *dlg*$^{40.2}$ mutant larvae (*dlg*$^{40.2}$*;lpp>*) expressing a *ctrl-IR*, an *imd-IR* or a myd88-IR in the fat body and representative immunofluorescence images of tissues quantified (I-K'). L-O, Quantification of TV (L, N) and TCD (M, O) from *dlg*$^{40.2}$ mutant larvae (*dlg*$^{40.2}$*;lpp>*) expressing a *ctrl-IR*, an *imd-IR* alone or in combination with a *UAS-def* in the fat body (L, M) and from *dlg*$^{40.2}$ mutant larvae (*dlg*$^{40.2}$*;lpp>*) expressing a *ctrl-IR*, a *myd88-IR* alone or in combination with a *UAS-def* in the fat body (N, O). Scale bars=50 µm. Statistical analysis: A, Student t-test, A, ***p=0.0001; B, C, Mann-Whitney test, B, ***p=0.0003, C, ***p=0.0002; F, G, H, L-O, One way ANOVA, *p<0.05, **p<0.01, ****p<0.0001.

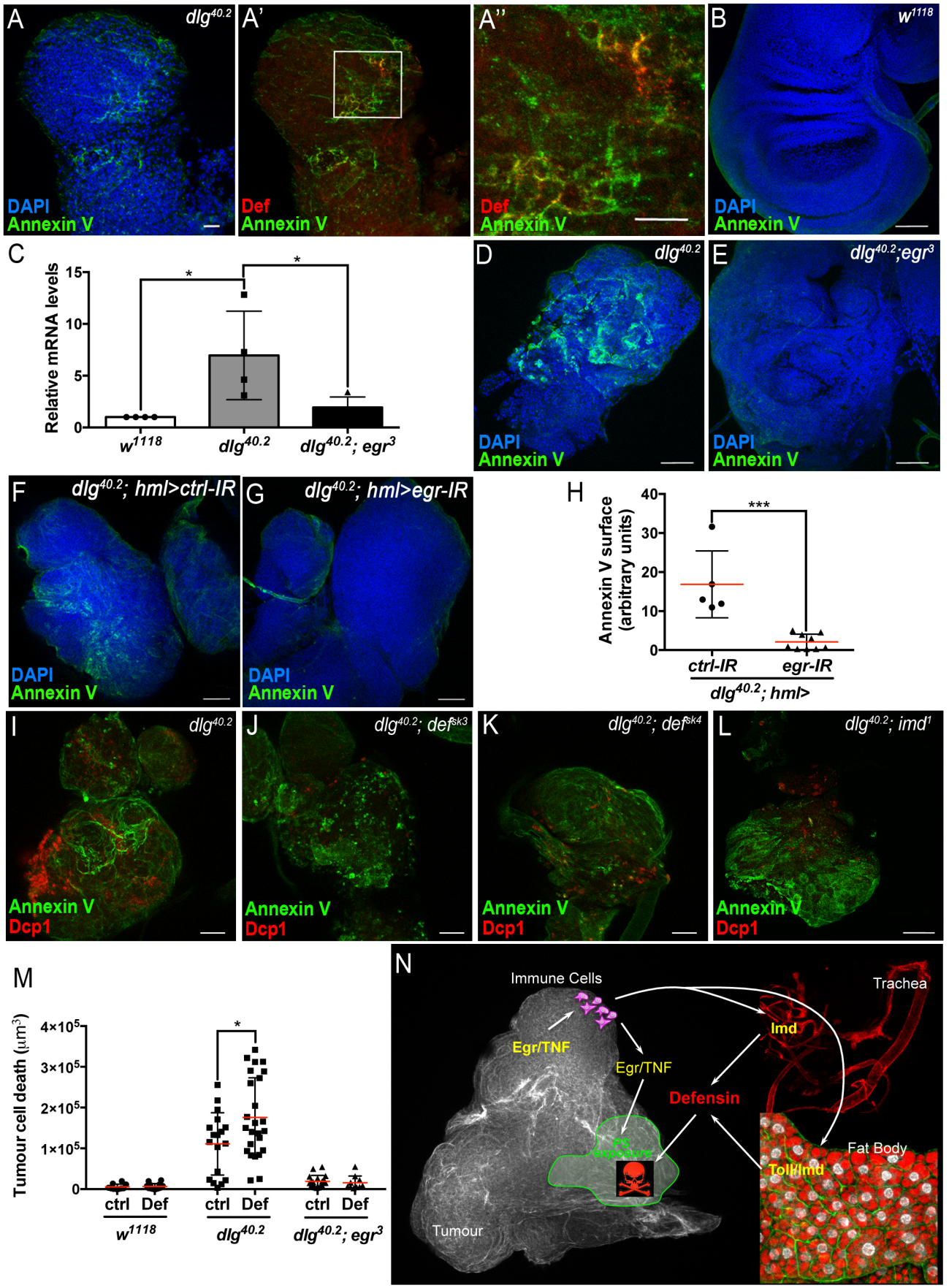
A
dlg40.2
DAPI
Annexin V
A'
Def
Annexin V
A''
Def
Annexin V
B
w1118
DAPI
Annexin V
C
Relative mRNA levels
15
10
5
0
*
*
w1118
dlg40.2
dlg40.2; egr3
D
dlg40.2
DAPI
Annexin V
E
dlg40.2;egr3
DAPI
Annexin V
F
dlg40.2; hml>ctrl-IR
DAPI
Annexin V
G
dlg40.2; hml>egr-IR
DAPI
Annexin V
H
Annexin V surface (arbitrary units)
40
30
20
10
0
***
ctrl-IR
egr-IR
dlg40.2; hml>
I
dlg40.2
Annexin V
Dcp1
J
dlg40.2; defsk3
Annexin V
Dcp1
K
dlg40.2; defsk4
Annexin V
Dcp1
L
dlg40.2; imd1
Annexin V
Dcp1
M
Tumour cell death (μm3)
4×105
3×105
2×105
1×105
0
*
ctrl
Def
ctrl
Def
ctrl
Def
w1118
dlg40.2
dlg40.2; egr3
N
Immune Cells
Trachea
Egr/TNF
Egr/TNF
Imd
Defensin
Fat Body
Toll/Imd
Tumour

Figure 7

Figure 7 | TNF is required for PS exposure and Defensin-driven tumour cell death. A-A'', DAPI (blue), Annexin V (green) and anti-Def (red) staining of *dlg*$^{40.2}$ mutant tumours. B, D, E, Annexin V (green) and DAPI (blue) staining of wing imaginal discs from larvae of the indicated genotypes. C, RT-qPCR analysis showing *def* expression in wild-type, *dlg*$^{40.2}$ or *dlg*$^{40.2}$*;egr*^{3} mutants. F, G, Annexin V (green) and DAPI (blue) staining of wing imaginal discs from *dlg* mutant larvae (*dlg*$^{40.2}$*,hml>*) expressing a *ctrl-IR* (n=5) or an *egr-IR* (n=9) in the haemocytes. H, Quantification of Annexin V signal on tumours from the corresponding genotypes. I-L, Annexin V (green) and anti-Dcp1 (red) antibody staining of tumours from *dlg*$^{40.2}$, *dlg*$^{40.2}$*;def*^{sk3}, *dlg*$^{40.2}$*;def*^{sk4} and *dlg*$^{40.2}$*,imd*^{1} mutant larvae. M, Quantification of TCD upon PBS (ctrl) or Def injection in wild-type (*w*^{1118}, ctrl: n=10, Def: n=14), *dlg*$^{40.2}$ (ctrl/Def: n=18) or *dlg*$^{40.2}$*;egr*^{3} (ctrl: n=20, Def: n=13) mutant larvae. N, A model for Def antitumoural activity. Scale bars=50 µm. Statistical analysis: C, One way ANOVA, *p<0.05; H, Mann-Whitney test, ***p=0.001; M, Two way ANOVA (only relevant significant statistics are indicated), **p<0.01.